JOURNAL OF GEOPHYSICAL RESEARCH, VOL. 105, NO. B3, PAGES 6127–6139, MARCH 10, 2000

Quasi-static fault growth and cracking in homogeneous brittle rock under triaxial compression using acoustic emission monitoring

Xinglin Lei[1] and Kinichiro Kusunose

Earthquake Research Department, Geological Survey of Japan, Tsukuba, Japan

M. V. M. S. Rao

National Geophysical Research Institute, Hyderabad, India

Osamu Nishizawa

Geophysics Department, Geological Survey of Japan, Tsukuba, Japan

Takashi Satoh

Earthquake Research Department, Geological Survey of Japan, Tsukuba, Japan

Abstract. This paper describes the localization of deformation acceleration in the period prior to dynamic failure in hornblende schist rock under triaxial compression using acoustic emission (AE) monitoring. Rather than stabilize the failure process by controlling axial stress to maintain a constant rate of AE (for monitoring AE hypocenters) as in previous works [e.g., *Lockner et al.*, 1991], we have instead developed a rapid multichannel data collection system. This enables us to elucidate the dynamics of fault nucleation under condition of constant stress (creep) loading, which is a better approximation to low strain rate condition in the Earth and allows both quasi-static and dynamic crack growth to occur. The waveforms of more than 8000 AE events which occurred mainly during a 15 s period were recorded on 32 channels, with a sampling rate of 50 ns and mask time of 200 μs. Hypocentral locations of AE sources revealed that the fault initiated at one end of the core and then propagated into the unfaulted rock with a process zone (fault front) of intense cracking. We found that there were two different processes operating during the quasi-static nucleation of a shear fault, namely, a process zone in front of the fault tip and a "wake" of damage zone following the process zone. The process zone had the following features: (1) major tensile cracking, (2) low b value and fewer larger events, and (3) strong self-excitation. The mechanism of crack interaction and fault growth was, therefore, a mutual enhancement on dilatation due to tensile cracking. On the other hand, the damage zone was characterized by (1) major shear cracking, (2) low b value and more larger events, and (3) weak self-excitation, indicating that in the damage zone, following the development of a shear fault, linkage between cracks became the major mechanism of crack interaction and fault development. The mutual changes of b value and self-exciting strength observed in our experiments seem to occur as a result of the hierarchy of fault growth, which was not observed under slowed down loading conditions. Therefore our experimental results, under a realistic approximation of the dynamic condition of the Earth, are meaningful for the problems of earthquakes as well as rock bursts.

1. Introduction

Controlled laboratory experiments of rock fracture and friction and the analyses of accompanying acoustic emissions (AE) are considered very useful for understanding and explaining the various mechanisms of stable and unstable failure of rock. Experiments aimed at investigating failure zone development and fault growth under natural loading conditions, i.e., when failure is allowed to develop unstably, have become possible and also more significant in recent years following the technological advances made in AE location and experimental loading methods [e.g., *Lockner et al.*, 1991; *Moore and Lockner*, 1995; *Kusunose*, 1995; *Lei et al.*, 1998; *Zang et al.*, 1998]. Such an endeavor is particularly useful in the study of the source physics of natural events such as earthquakes and rock bursts, since large-scale testing of rock in the field is not easy. Rock-fracturing experiments of intact brittle rocks have produced useful results since the late 1960s for the investigation and modeling of fault formation and growth in

[1] Also at Institute of Geology & Laboratory of Tectonophysics, China Seismological Bureau, Beijing, China.

Paper number 1999JB900385.
0148-0227/00/1999JB900385$09.00

rock. Early studies postulated that faults were formed by the coalescence of arrays of cracks which nucleated from preexisting damage sites [*Brace et al.*, 1966; *Scholz*, 1968; *Horii and Nemat-Nasser*, 1985]. However, recent experimental results have demonstrated that cracks occurring at or near the yield stress in a homogeneous granite actually have hardly any effect on the geometry and location of the future fault [*Moore et al.*, 1990; *Lockner et al.*, 1991; *Lockner and Byerlee*, 1993]. Experimental results on fine-grained granites have invariably shown that faults nucleate and propagate by the interaction of tensile cracks [*Reches and Lockner*, 1994; *Moore and Lockner*, 1995]. However, *Cox and Scholz* [1988] conducted a torsional experiment and pointed out on the basis of microscopic examination that mainly tensile cracks were formed in the dilatant-hardening phase with major failure occurring because of shear crack formation by cracking. Using a direct focal mechanism solution using *P* wave first motions detected by 20 AE sensors, *Lei et al.* [1992] found that the tensile cracks in fine-grained granite were dominant only until the yield point, after which shear cracks dominate until failure. On the other hand, shear cracks were present dominantly throughout the loading history of coarse-grained granite.

Many experimental studies on the frictional behavior of a well-prepared fault plane in rock have also led to important results. For example, the fracture nucleation model proposed by M. Ohnaka and others [*Ohnaka*, 1996; *Dieterich and Kilgore*, 1996] is mainly based on high-resolution laboratory friction experiments [*Dieterich*, 1992; *Ohnaka and Kuwahara*, 1990; *Ohnaka and Yamashita*, 1989]. According to that nucleation model the earthquake generation process can be considered as a transition process from a quasi-static nucleation to a dynamic rupture [*Ohnaka*, 1996]. Crack growth in the quasi-static nucleation process occurs at a very low velocity ranging from cm/s to m/s [*Ohnaka*, 1996; *Kato et al.*, 1992]. When the crack length becomes critical, it propagates very fast at a velocity approximately equal to V_s (velocity of shear wave in rock), leading to dynamic rupture. As a result, both fracture of intact rock and friction of fault show a process from quasi-static nucleation to dynamic rupture.

Although most shallow earthquakes are usually assumed to occur on preexisting faults, the fracturing process of intact rock is as important as the friction of the fault for understanding the quasi-static nucleation of a natural fault. If a fault or some parts of the fault are healed, then it is a prerequisite that the healed parts must fracture first before the dynamic slip occurs on that fault. Further, earthquake faults are indeed fault zones of a finite width, ranging approximately from a few tens of meters to several hundreds of meters, and the fault rupture is not a distinct slip across a simple fault plane but rather a shear zone [*Johnson et al.*, 1994; *Li et al.*, 1994]. A fault zone is a very complex system having many individual subfaults, junctions, bends, and other geometrical complexities. In such a case, for the quasi-static nucleation phase, both friction and fracturing (or microfracturing) are important. The detection and analysis of the quasi-static nucleation of a fault under loading conditions consistent with the Earth are quite important. Since a shear fault will be formed spontaneously before the rock fails, some precursory phenomena might be produced by such fracturing activity on a smaller scale. However, experimental studies traditionally carried out under constant strain rate loading control have been made difficult by the tendency for the fault to grow in an uncontrolled manner after its initiation at a relatively high strain rate achievable in the laboratory. Since there is a surge of cracking activity in a very short time (generally in seconds) during the nucleation and growth of a fault under these conditions, most experimental systems cannot detect enough AE data, especially waveform data.

However, there are some exceptions. For example, a nonstandard "asymmetric" compression test [*Zang et al.*, 1998] carried out under uniaxial compression facilitated earlier initiation and growth of the fault at a lower stress. Using AE occurrence rate rather than strain rate as a feedback signal to control the axial loading, *Lockner et al.* [1991] were successful in investigating the quasi-static growth of a fault in granite and sandstone samples through the analysis of AE hypocenters. However, as we know, the constitutive relation of friction [e.g., *Dieterich*, 1992] and the mechanics of the interaction between cracks are indeed time-dependent, so the fault growth under artificially slowed down conditions with time-varying strain rate may not be completely representative of the dynamic loading conditions in the Earth. As an alternative, we have studied cracking activity during the spontaneous, quasi-static growth of a fault in intact rocks using a new fast AE waveform recording system that can record as many as 8000 AE waveforms on 32 channels with a mask time of 200 μs [*Satoh and Nishizawa*, 1997; *Lei et al.*, 1998]. In other words, rather than slow down the process using AE event rate as in previous work [e.g., *Lockner et al.*, 1991], we have previously used this system for our AE monitoring experiments. The main advantage of our new method as compared to AE feedback is that the process of fault growth is in a condition of constant stress (creep) loading, which is a better approximation to low strain rate condition in the Earth. Therefore we expect that our experimental results are more meaningful to the problems of earthquakes and rock bursts.

In this study, three core samples of hard and homogeneous brittle hornblende schist rock of the Kolar Gold Mine, India, at a depth of 730 m, where mine-induced seismicity and microseismicity are very active, were chosen for testing. The laboratory and field monitoring studies were planned and performed to investigate the microseismicity of these burst-prone rocks at different scales, as a part of the work on rock burst research in the deep mines of the Kolar Gold Field [*Rao*, 1996; *Satoh et al.*, 1996]. The hornblende schist rocks have a maximum grain size of 0.7 mm and are more homogeneous than typical granites, which have been used for many experiments. Since low AE activity before peak strength can be expected, it is easy to distinguish cracking in the fault nucleation zone from background activity.

2. Experiment

We used a hornblende schist collected from the Kolar Gold Mine as mentioned in section 1. The test samples (100 mm long and 50 mm in diameter) have a modal composition of 60% hornblende, 20% quartz, 12% plagioclase, and 8% other minerals. The grain size ranged from 0.2 to 0.7 mm; thus the rock is more homogeneous than typical granite such as Oshima granite and Westerly granite. The rock collected at the field site is not oriented. Therefore the direction of schistosity with respect to the principal stress direction of the field is not known. Schistosities in the test samples are oriented in a direction having an angle of ~80° relative to the axial direction. Therefore the schistosity may not control the final fracture

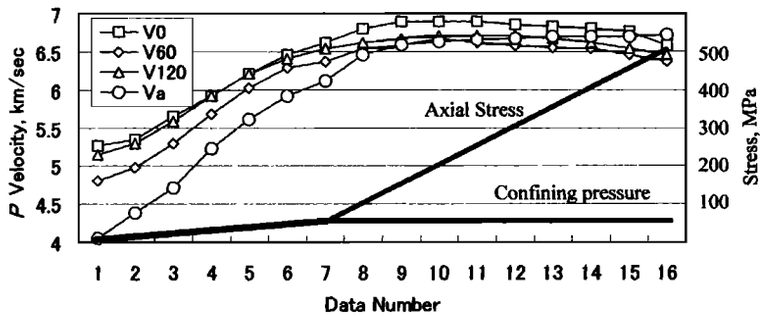

Figure 1. Velocities V of P wave measured along four typical directions during the experiment. V_0, V_{60}, and V_{120} were measured along three diameter directions of an azimuth angle of 0°, 60°, and 120°, respectively. V_a was measured along the axial direction of the sample. Axial stress and confining pressure are also plotted in Figure 1.

plane, though it may affect the fracture process. We measured the P velocities of the test sample along many directions before and during the experiments. Figure 1 shows the measured velocities along four typical directions. Velocity anisotropy, V_{max} - V_{min}, was ~1.3 km/s at a low stress level. However, it decreased gradually with increasing confining pressure and axial stress. Finally, when the confining pressure was kept constant at 60 MPa, the velocity anisotropy became almost constant around 0.5 km/s.

A functional block diagram of the experimental setup along with important details of the loading and AE recording systems is shown in Figure 2. The main advantages of the AE recording system are as follows: (1) The system has a fast waveform recording facility on 32 channels with a selection of sampling rate up to 25 MHz and dynamic range of 12 bits. (2) The mask time of our system is <200 μs, thus making it possible to record AE waveforms without any important loss, particularly when the AE activity is very high, on the order of a few thousand events per second. (Any waveform recording system has a mask time for transmission of data after a trigger signal is detected. The system is in a frozen state and thus cannot record any new signal during the period of the data transmission.) (3) The system has a two-channel detector to capture the values of peak amplitudes up to the 99 dB dynamic range. Since the noise level after passing through a 20 dB preamplifier is generally around 45 dB, the effective dynamic range for AE signal is 55 dB, which corresponds to a magnitude range of ~2.75. Further, since the peak detector shares a common base clock with the waveform recording system, it is possible to obtain a complete set of temporal and spatial distributions of AE events. The details of the system are described elsewhere [*Satoh and Nishizawa*, 1997; *Lei et al.*, 1997, 1998].

In all, 32 piezoelectric transducers (PZT) of 2 MHz resonant frequency were mounted on the curvilinear surface of the test sample and two end faces as shown in Figure 3. The PZT transducers function not only as receivers of acoustic signals but also as acoustic sources for measuring the velocity of the P wave during the deformation of the rock. Changes between being a receiver and detonator are controlled by a number of automatic switches. Six pairs of X-type strain gages were fixed in the middle on the curvilinear surface of the test sample (in Figure 3). All data, including waveforms, peak amplitude values, and stress-strain data were collected by a real-time AE hypocenter monitoring software [*Lei et al.*, 1998]. AE hypocenters were determined automatically by using the first arrival time data of P waves and measured P velocities.

In total, we have completed three tests. The first experiment, referenced as KO980325, is used mainly for measurement on the strength of the rock, but some data were not recorded. The other two tests, referenced as KO980401 and KO980408, are loaded in a similar way to check consistency. In fact, the important experimental results of the three tests such as stress-strain curve, AE rate, pattern of AE hypocenters, and fracture orientation are consistent with each other, although some details are different. Therefore we will discuss mainly the results of KO980401, but some data of KO990408 are also used to show consistency. The confining pressure was set at 60 MPa and held constant throughout the experiment. As mentioned above, the samples were very brittle and homogeneous. We could not estimate the exact strength of the sample during experiments using AE rate or stress-strain curve. Therefore there is no way to find the best stress level to start creep. If the stress for creep is too low, the rock may never fail. On the other hand, if the rock was overloaded, it might fail unexpectedly. To avoid these results, a step loading was applied. In the case of KO980401 the sample was loaded axially at a constant rate of 0.05 MPa/s until ~660 MPa; thus the differential stress was 600 MPa when the load was held constant over 30 min. Since no AE activity occurred and there was no obvious change of strain, the load was increased two more times. Finally, loading was kept constant at 710 MPa (differential stress of 650 MPa), as shown by the loading histories in Figures 4a and 4b. On the basis of experimental results of KO980401, KO980408 was loaded at a constant rate of 0.05 MPa/s until 710 MPa, and then the load was kept constant.

Figure 4 also shows plots of axial stress, strain, and AE occurrence rate versus time. The samples finally failed dynamically under constant loading or "creep" conditions (σ_A = const). There was no clear phase between yield point and peak strength. In fact, the stress-strain relation is almost linear immediately before final fracturing, which is typical of the hard homogeneous and brittle rocks of the Kolar gold mines. There was no obvious AE activity until the peak stress was approached. However, rapidly increasing AE activity was detected during this time interval (15 s). For each experiment a total of more than 20,000 AE events could be recorded for determining the peak amplitudes, and ~8000 events were recorded with waveforms. Since the trigger level for the waveform recording system was higher than the peak detector, the AE events recorded with waveform were a subset of the larger number of events recorded by the peak detector.

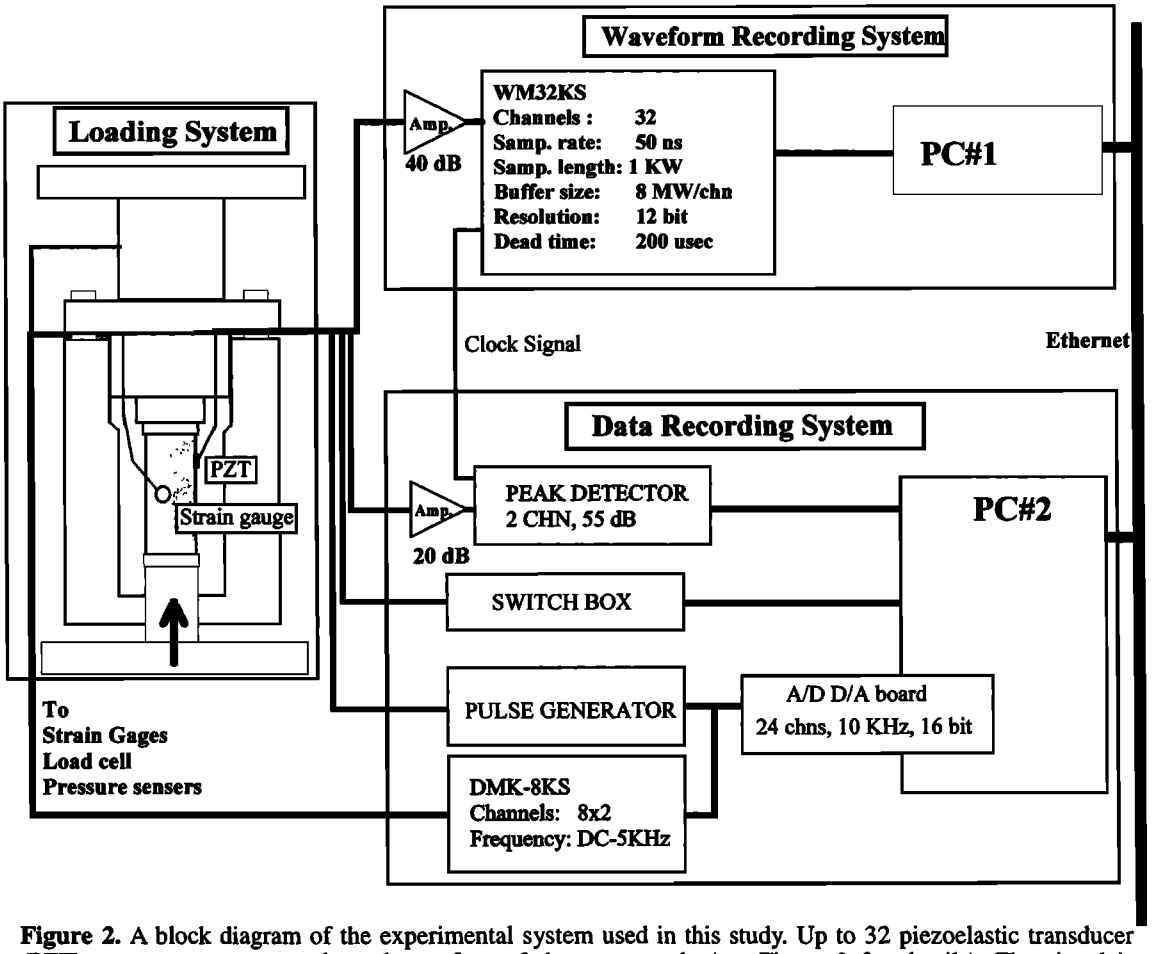

Figure 2. A block diagram of the experimental system used in this study. Up to 32 piezoelastic transducer (PZT) sensors were mounted on the surface of the test sample (see Figure 3 for details). The signal is preamplified by 40 dB before feeding into a fast waveform recording system which has a maximum sampling rate of up to 40 ns and a dynamic range of 12 bits. A two-channel peak detector was used to capture the values of the peak amplitudes after 20 dB preamplifiers. An automatic switch box was used for switching some sensors between AE measurement and velocity detecting during the experiment. Stress, strain, and confining pressure were recorded using two 16-bit analog to digital (A/D) boards.

Figure 5 shows an example of typical AE event waveforms recorded on 32 channels, with the letters A and P indicating autodetected and calculated arrival times, respectively, using the hypocenter determination program. The estimated location error for most AE events is <2 mm [*Lei et al.*, 1992]. The hypocenters of >50% of the events recorded were determined precisely. The temporal and spatial distribution of AE hypocenters projected in the axial direction of the sample along with a trace of the main fault formed in the test sample KO980401 are shown in Figures 4c and 4d. Most hypocenters are found to occur in the main fault, which is a slightly curved three-dimensional plane having a dip angle of ~15°-20°. As mentioned in section 1, the schistosity of the samples has an angle of 80° with respect to the axial direction. The main fault was not controlled by the schistosity of the sample.

3. Data Analysis

The mechanics of brittle deformation and crack growth can be inferred from AE statistics, because the number of AE events is proportional to the number of growing cracks and AE amplitudes are proportional to the length of crack growth increments in rock [e.g., *Main et al.*, 1989, 1993; *Sun et al.*, 1991; *Cox and Meredith*, 1993; *Rao*, 1996]. The well-known *Gutenberg-Richter* [1954] relationship,

$$\log_{10} N = a - bM , \tag{1}$$

where N is the number of events of magnitude M or greater, holds true for not only earthquakes but also AE events in rock samples [e.g., *Liakopoulou-Morris et al.*, 1994; *Scholz*, 1968]. In (1), a is a constant, and b is the seismic b value. An estimate of the b value in the *Gutenberg-Richter* relation can be obtained by using either the least squares method or the maximum likelihood method [*Utsu*, 1965], which yields

$$b = \frac{N \log_{10} e}{\sum_{i=1}^{N} (M_i - M_c + c)}, \tag{2}$$

where M_c is the cutoff magnitude and c is the justification constant equal to half the difference between successive magnitude units, which is 0.25 for our data (thus c=0.125). The approximate standard error of the b value estimation is $\sigma = b/\sqrt{N}$ [*Aki*, 1965].

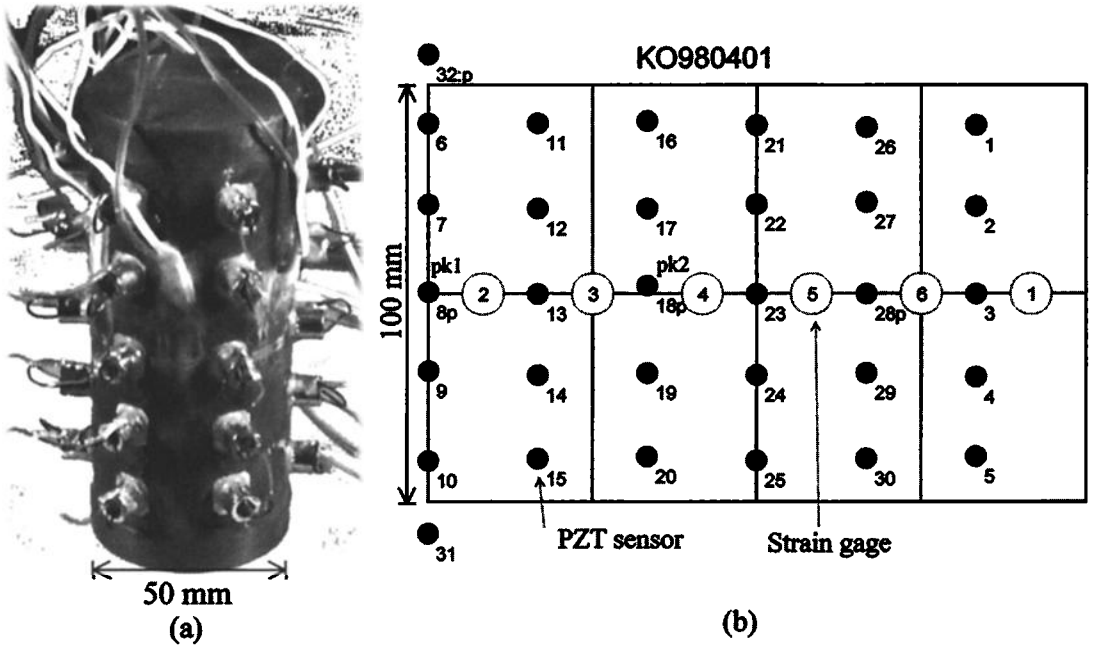

Figure 3. (a) Photograph of rock sample used in this study. (b) Location map of 32 PZT sensors and six cross-type strain gages. There were 30 PZT sensors (sensors 1-30) mounted on the surface of the rock sample. Two other sensors (sensors 31 and 32) were mounted on the two end pieces. Signals from sensors 8 and 18 were also fed to the peak detector. Confining oil was prevented from infiltration into the rock sample by encapsulation in silicone of 3-5-mm thickness.

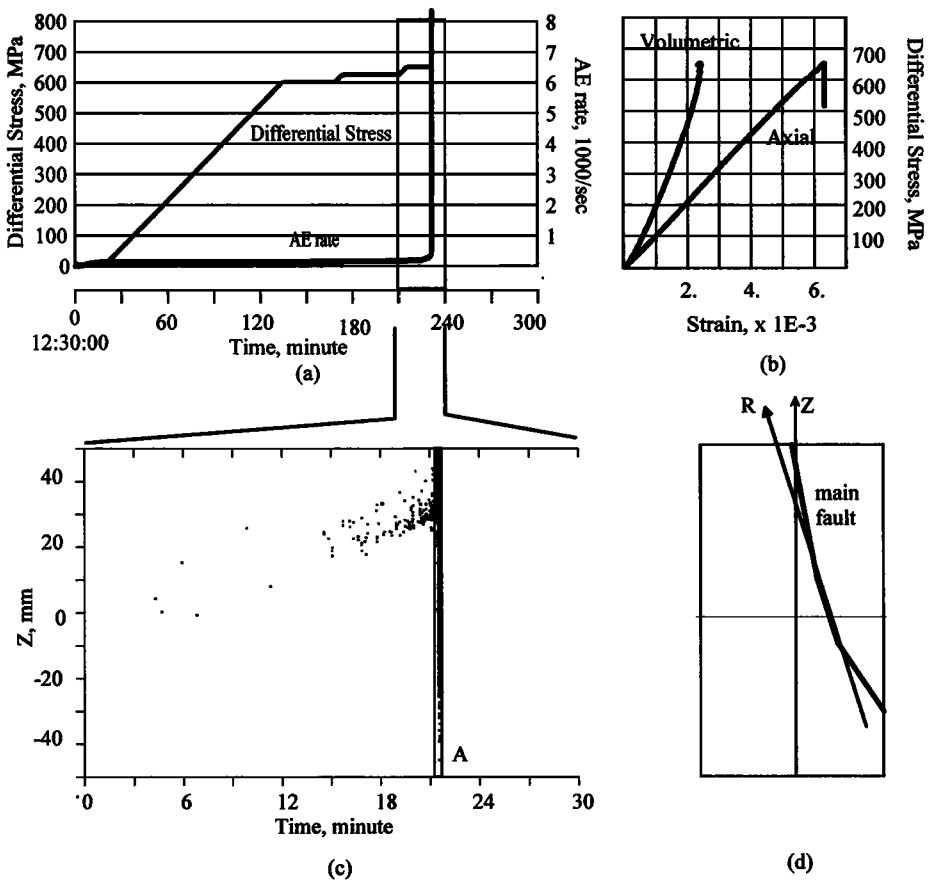

Figure 4. (a) Plot of differential stress and cumulated AE occurrence rate against time. (b) Differential stress against average axial strain and volumetric strain. Read 2x1E-3 as $2x10^{-3}$(c) A temporal-spatial distribution of AE hypocenters projected in the dip direction of the main fault (*R*). A indicates the period of the quasi-static growth of the main fault. (d) A vertical profile of the sample with the main fault.

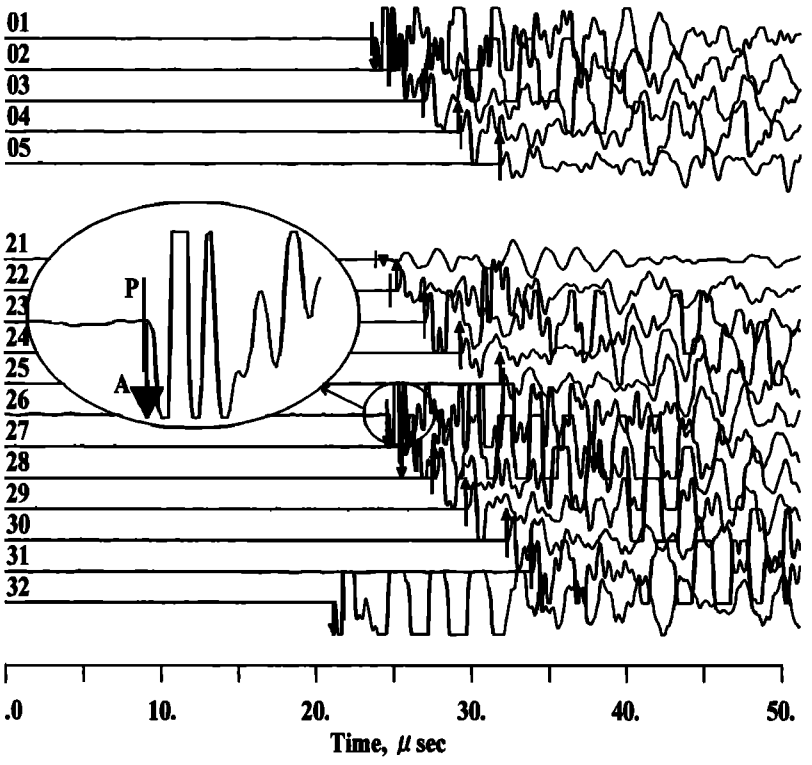

Figure 5. Waveforms of a typical AE event. The vertical lines marked as A and P indicate the arrival times autodetected from waveform and calculated from location data, respectively. The arrow indicates the autodetected polarization direction.

AE events did not occur randomly, but rather had a time-dependent probability distribution. To analyze AE occurrence in time, *Nishizawa and Noro* [1990] applied a self-exciting (or "triggering") model, which was originally proposed by *Ogata et al.* [1982] for analyzing earthquake data. *Nishizawa and Noro* [1990] reported that the impulse function of the self-exciting model, which indicates the probability of excitation of preceding events on succeeding events, was enhanced under higher crack density. We expected that the self-exciting model would be useful for modeling the cracking activity during the quasi-static fault growth in the homogeneous rock that we have studied.

We used the following conditional function for describing the instantaneous probability of AE occurrence [*Ogata et al.*, 1982, *Nishizawa and Noro*, 1990]:

$$\lambda(t) = \mu_0 + \sum_{j=1}^{J} p_j t^j + \sum_{t_i<t} g(t-t_i), \tag{3}$$

where μ_0 is the constant expressing the stationary Poisson process, $p_j t^j$ is the function expressing a trend or cyclic component, t_i is the occurrence time of the ith event, and $g(t)$ is the impulse response function used to express excitation on succeeding events. The $\lambda(t)$ is the same as the failure rate or risk function used for expressing the system reliability. The following Laguerre polymial is used for expressing the impulse function $g(t)$, because this function is consistent with the causality inherent in a triggering process and can also easily make the calculation of the likelihood function, which is used for selecting the optimum model parameters, tractable.

$$g(t) = \sum_{m=0}^{M-1} a_m t^m e^{-\beta t} \tag{4}$$

For time series data $\{t_i, i=1,2,\ldots,N\}$ in the time interval $[0, T]$, the likelihood of the model defined in (3) is given as [*Ogata and Katsura*, 1986]

$$L_\theta = \{\prod_{i=1}^{N} \lambda(t_i)\} \exp\{-\int_0^T \lambda(t)dt\}, \tag{5}$$

where expresses the parameters of the model, say, $\theta\{\mu_0, p_1, p_2, \ldots, p_J, J, a_0, a_1, \ldots, a_{M-1}, M, \beta\}$. On the basis of the statistic theory the quality of the parameter values of a specific model can be measured by the expected log likelihood; namely, the larger the expected log likelihood, the better the values of parameters. The maximum likelihood, however, is shown to be a biased estimator of the mean expected likelihood. The maximum likelihood has a general tendency to overestimate the true value of the mean expected log likelihood. Therefore Akaike's information criterion (AIC), defined as the following, is proposed as the criterion for model selection [*Akaike*, 1974]:

$$\mathrm{AIC} = -2 \max(\log L) + 2N_p, \tag{6}$$

Where L is the likelihood and N_p is the number of parameters. A model which minimizes the AIC is considered to be the most appropriate model. AIC penalizes additional parameters, it is best to produce the simplest model consistent with the data.

We have developed an easy-to-use visual program for finding the optimum model parameters and calculating the b

Table 1. An Example of Model Parameters

Model	μ_0	p_1	p_2	a_0	a_1		AIC
Poisson	0.1374						2987
Trend	0.1258	-4.34E-5	2.05E-8				2950
Self-exciting 1	0.0971			0.0417		0.1392	2943
Self-exciting 2	0.0969			0.0418	0.1395	0.1374	2945

Model of the minimum AIC is assumed to beoptimum. Model parameters μ_0, p_1, p_2, a_0, a_1, and β are defined in (3) and (4). AIC, Akaike's information criterion. Read –4.34E-5 as -4.34×10^{-5}.

value. For checking the temporal changes of model parameters and b value the optimum model and b value were estimated using a running window of $N = 500$ events and a running step of 125 events. Table 1 shows the results of parameters and AIC values of typical models, a Poisson model (J=0, M=0; i.e., g(t)=0), a trend model (J>0, M=0), and a self-excitation model (M>0). The self-exciting model run with J=0 and M=1 (Self-exciting 1 in Table 1) has the minimum AIC and thus indicates the optimum model. For most data sets a model of parameter set $\{\mu_0, a_0, \beta\}$ (in other words, $J = 0$ and $M = 1$ in (3)) has the minimum AIC value. This result suggests that AE occurrence can be modeled best by the combination of a standard Poison process and self-exciting process. There are also few exceptions when the AE rate obviously changed in the data window. This time a model of J>0 and M=1 became the best model. Anyway, for all data the impulse function is the same as $g(t) = a_0 e^{-\beta t}$. Therefore the integration of the impulse function $g(t)$,

$$s = \int_0^\infty g(t)dt = \int_0^\infty a_0 e^{-\beta t}dt = \frac{a_0}{\beta}, \quad (7)$$

is a value expressing the strength of the excitation of the preceeding event on succeeding events, or, equivalently, the degree of positive feedback in the dynamics. Thus the temporal changes of a_0/β and the b value are the key data in this study.

4. Results

Figures 6-10 show the basic results of our experiments. In Figure 6, cumulated AE numbers calculated from peak data and waveform data, self-exciting strength a_0/β, and b value are plotted against time. AE hypocenters projected in the axial direction of the sample are also plotted against time. Note that in the time window shown, which is 50 s and indicated by A in Figure 4, there was hardly any induced change in loading and confining pressure; that is, these were essentially

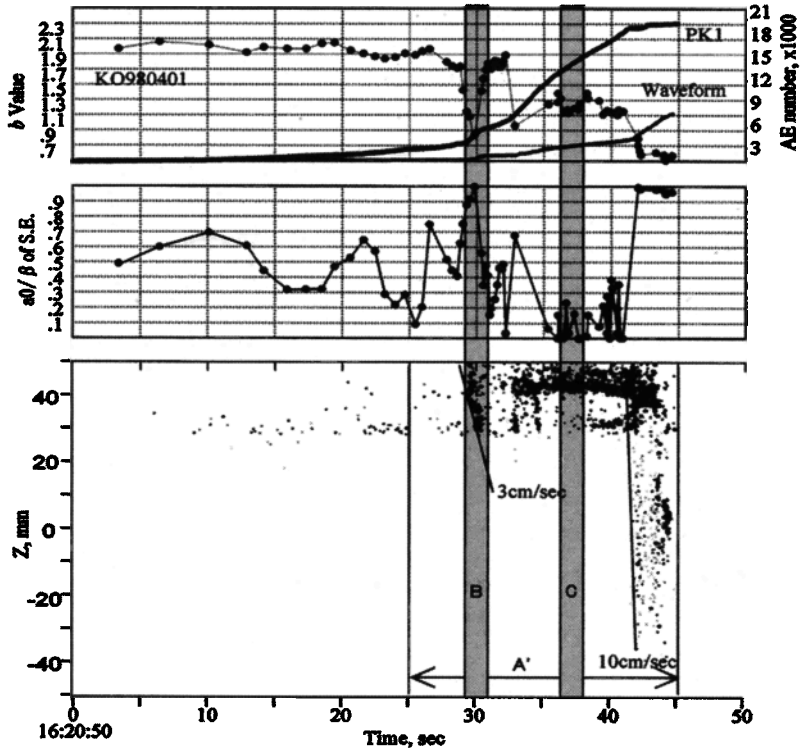

Figure 6. Results of KO980401. Plots of cumulated AE numbers and b values calculated from maximum amplitude data (PK1, at PZT sensor 1) and waveform data, self-exciting (S.E.) strength (a_0/β) of the estimated optimum model, and AE hypocenters projected in the axial direction of the sample. All plots are marked against a uniform time axis.

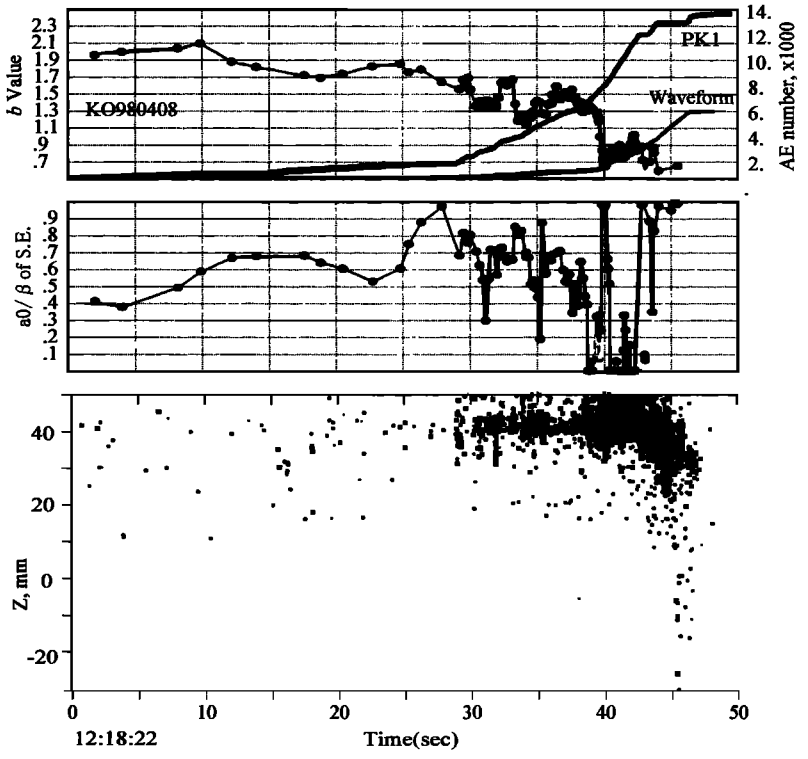

Figure 7. Results of KO980408.

creep-to-failure conditions. Figure 7 shows the results of KO980408, which are similar to these of KO980401 as plotted in Figure 6, except for some details.

4.1. Temporal and Spatial Distribution of Cracking

Since an AE event generally corresponds to a cracking, the AE hypocenter distribution reflects directly the distribution of cracking in rock under stress. Overall, the cracking is distributed on or around the main fault, which is a slightly curved three-dimensional plane. Fault initiation and growth were monitored closely using AE hypocenter distribution data in our study. Before the rapid increase of AE activity there were few AE events, which started in the center of the sample and migrated to the top end. Then the fault initiated there and propagated spontaneously in its own plane with a process zone (in other words, a front area of the fault) of intense cracking. After the fault front passed through, the nucleation zone (hereafter, we note it as a damage zone for comparison with the process zone) had generally high cracking activity, which was not uniform but rather shows some clustering. The time interval between the initiation of the fault and dynamic rupture of the final fracturing is ~15 s.

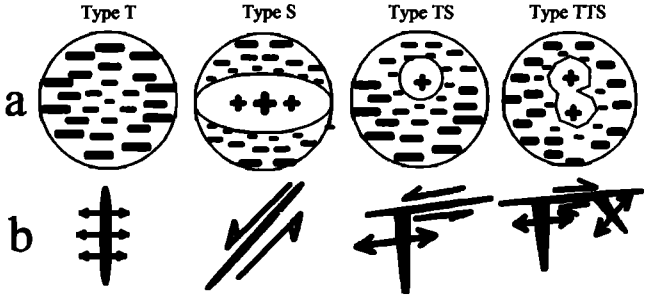

Figure 8. Four types of focal mechanism solution observed in our experiment. (a) Distribution of the first *P* wave motions on an equal-area projection of the lower hemisphere of the focal sphere. (b) Cracking modes corresponding to Figure 8a. See text for details.

Generally, migration velocity of cracking does not indicate the velocity of rupture growth directly. However, the migration of the front of rapidly increasing cracking along the failure plane in the short time prior to the dynamic rupture can be reasonably considered as a quasi-static rupture velocity. As shown in Figure 6, the growth of the fault nucleation can be divided into two stages. First, the fault nucleation grew to ~2 cm at a speed of 3 cm/s along its dip direction (see also Figure 10 for details), and then the growth stopped for ~12 s even though cracking in the damage zone was still very high and showed clustering. At last, the fault nucleation grew to a size reaching the edge of the sample at a higher velocity, around 10 cm/s (Figures 5 and 10). It is interesting that the dynamic rupture did not occur immediately after the fault reached the edge of the sample, but rather there was a ~2 s delay. During this time interval, intense cracking occurred in the fault plane and was concentrated in some areas. Since events occurred frequently at this moment, waveform signals were noisy; thus many events could not be located with good accuracy. Therefore there is an apparent decrease of hypocenter density on the AE distribution map. This result shows that the fault nucleation formed and grew gradually with increasing crack density. The dynamic rupture occurred when the crack density in the fault nucleation zone reached a critical value.

Using the fault growth velocity and time interval between the last quasi-static growth and dynamic rupture (Figures 6 and

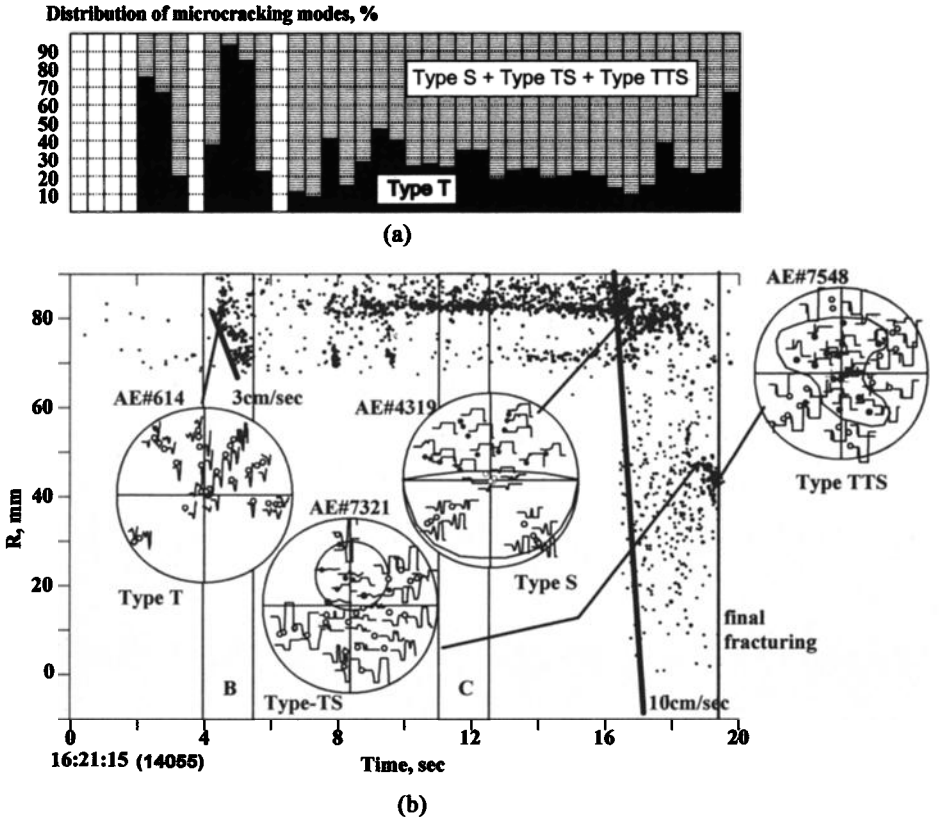

Figure 9. (a) Temporal change of cracking modes estimated using the first motion polarization data (see text for details). (b) Temporal change of AE hypocenters projected in the dip direction *R* of the main fault as defined in Figure 3. Typical focal mechanism solutions are also plotted. B and C indicate a typical process zone and a typical damage zone, respectively. Note that the time window shown is 20 s and is indicated as A' in Figure 6.

7), a critical nucleation size can be estimated, which is approximately 10 cm/s x 3 s, say, 30 cm. This size is larger than the dimension of the sample; thus it is not an observed fact but only a simple estimation. Even through, the estimated critical size is between the results of friction experiments (of the order of millimeters to centimeters) and earthquakes (of the order of meters to kilometers) [*Cox and Scholz*, 1988].

4.2. Focal Mechanism Solution

Focal mechanism solutions are an important clue for determining the modes of cracks [e.g., *Sondergeld and Estey*, 1982]. In our experiments, four types of mechanism solution were distinguished using the distribution of *P* wave first motions. We have categorized them as type T, type S, type TS, and type TTS, respectively, for convenience. Figure 8 is a schematic illustration showing the distribution of the first motions and the likely corresponding crack modes. Type T, which corresponds to tensile cracking, has compressional first motion at all sensors. Type S having quadrantal distribution of *P* wave first motion, is generated by a shear cracking. Type TS is assumed to be a slip along the crack with tensile cracking at its end (it is also called wing crack [*Ashby and Sammis*, 1990]). Type T, type S, and type TS have been observed in many other experiments [e.g., *Zang et al.*, 1998; *Lei et al.*, 1992]. Type TTS is reported here for the first time. As shown in Figure 9, AE 7548 is the polarization distribution of a typical type TTS event. Every receiver has a clear first motion, but the distribution of polarization cannot be assigned to either type S or type TS cracks. However, it may be modeled by a slip along a crack with two tensile cracks of different orientations at its ends. In other words, the combination of two type TS cracks.

The distribution of the four cracking types is not uniform. We used a ratio between up (dilatational) and down (compressional) first motions to distinguish between type T and other types. The ratio is defined as up/(up+down). To maintain good reliability, only those data having (up+down)>7 were used. By comparing the result by manual checking, we assign a cracking of up-down ratio <0.25 and >0.25 to tensile mode and shear mode (including other modes having shear component), respectively. The distributions of cracking modes are plotted in Figure 9a against time. The AE hypocenters are projected in the dip direction R of the main fault as defined in Figure 4. A typical polarization distribution for each type is plotted in Figure 9b. We found that tensile cracking was dominant before and at the initiation stage of the main fault (see also Figure 10a). Cracking in the process zone, or, in other words, at the tip of fault, was also mainly in the tensile mode. However, in the damage zone the shear and wing crack modes became dominant, although tensile mode remained important to some extent (see also Figure 10a).

4.3. The *b* Value and Self-Exciting Model

In our tests the *b* value fluctuated during the fault growth (Figures 6 and 7). Before the initiation of the fault a high average *b* value of 2.0 was obtained. When the fault was

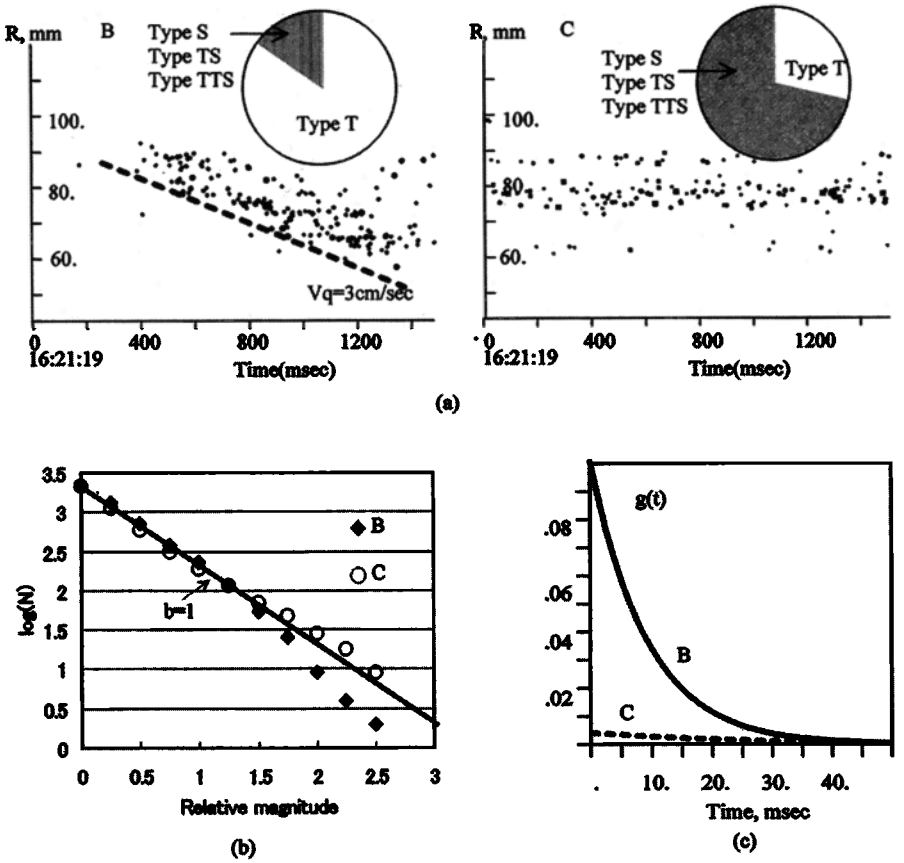

Figure 10. (a) A detailed view of the temporal and spatial distribution of AE hypocenters in a typical process zone (B) and typical damage zone (C), as defined in Figures 6 and 9. AE hypocenters are projected in the dip direction R as defined in Figure 4. Distributions of cracking modes are also shown in pie graphs. (b) Number-magnitude relations for B and C. Note that there are a greater number of larger events in C than in B. (c) The impulse function $g(t)$ of the self-excitation model of AE occurrence for B and C. Note that events in B show much stronger self-excitation than in C.

initiated, the b value decreased to ~1.2. When the fault stopped growing, the b-value rose again and then decreased to ~1.2 following the increase of crack density. At last, immediately before the final fracturing, the b value became as low as 0.5. However, at this stage, larger AE events with longer duration occurred frequently, while smaller events might have been masked or buried by larger ones, thus giving rise to an erroneous b value. The dual changes of the b value before the dynamic fracturing are similar to the "double-b-value" anomaly predicted by *Main et al.* [1989] and observed by *Sammonds et al.* [1993]. By comparing the b values with AE hypocenter data, this kind of double-b-value anomaly seems to occur as a result of the hiatus in fault growth. During the hiatus only background cracking occurs, which generally shows a higher b value.

The strength of self-excitation (a_0/β), as shown in Figures 6 and 7, shows also mutual changes during fault growth. It was particularly enhanced at the initiation stage of the fault and immediately before the final fracturing. In the damage zone self-excitation is rather weak. The change of self-exciting strength is comparable to b value. However, there is no clear correlation between the two values.

On the basis of our results on AE data we conclude that the quasi-static nucleation of a shear fault consists of two parts with different cracking behaviors: a process zone at the front of the fault and damage zone or "wake" following the process zone. In our experiments the fault growth paused temporarily for a while after its initiation, making it easy to find a typical process zone (B in Figures 6 and 9) and typical damage zone (C in Figures 6 and 9). The temporal and spatial distribution of AE hypocenters, number-magnitude relations, and $g(t)$ of the self-excitation model for B and C are shown in Figure 10. Both B and C show lower b values of ~1, but the larger events in C were more than B (Figure 10b). AE events in B show very strong self-excitation, but C did not (Figure 10c). Tensile cracking was dominant in B while shear cracking was dominant in C (Figure 8a).

5. Discussion

The differences between process zone and damage zone on the b value, cracking mode, and self-excitation suggest that the interactions between cracks in the two zones were different. As illustrated in Figure 11, we conclude that in the process zone a mutual enhancement on dilatation is due to tensile cracking as proposed by *Reches and Lockner* [1994]. It was the major mechanism of crack interaction and fault growth. Following the development of a shear fault in the damage zone, the linkage between cracks became dominant gradually. This conclusion is in agreement with the microscopic examination result on a torque test revealed by *Cox and Scholz* [1988].

Since it is a hard work to check all the waveform data for

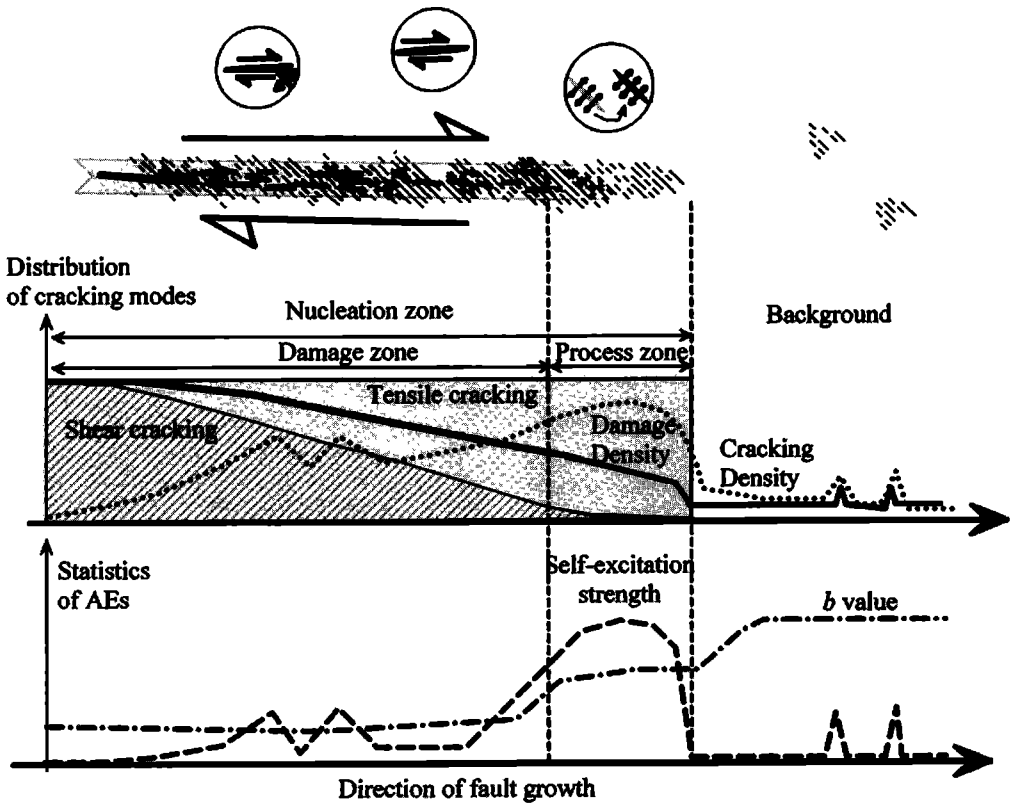

Figure 11. Schematic section through quasi-static growth of a shear fault, indicating successive generations and fracturing modes of cracks. The fault is growing toward the right. See text for details.

making exact focal mechanism solutions for several thousand events, our results on crack modes in the process zone and damage zone are not enough. In combination with microscopic examination it may make this process more clear. It is our future interest of study. It also requires that we improve our program for the selection of events between process zone and damage zone.

The growth velocities obtained from AE hypocenter migration are on the same order as that obtained from friction experiments at a slip rate of the order of 10^{-6} [*Ohnaka*, 1996; *Kato et al.*, 1992]. Does this mean that the constitutive relation obtained from friction experiments is also true for the fault growth in an intact rock? This is an interesting question, which needs further study.

The mutual changes of b value and also the strength of the self-exciting model seem to occur as a result of the hiatus in the fault growth. During the hiatus only background cracking occurs. Since cracking in the fault nucleation zone shows a low b value, and background activity shows a high b value, mutual changes of b value could be observed. Therefore the mutual changes of the b value also indicate a hierarchy of fault growth. This kind of hierarchy of fault growth was not observed under the loading conditions of constant AE rate [*Lockner et al.*, 1991].

The change of self-exciting strength is comparable to the b value. However, there is no clear correlation between the two values. Both the process and damage zones show a low b value. On the other hand, the process zone shows strong self-exciting, i.e., strong positive feedback, but the damage zone did not. Therefore a combination of the b value and self-exciting strength is quite useful.

Seismologists expected that the critical nucleation size, and thus the magnitude of potential earthquake, might be estimated using foreshock activity of microearthquakes. Our experimental results on the process zone and damage zone may be helpful in determining the physical basis for such endeavor.

6. Conclusion

We have investigated spontaneous fault nucleation and its quasi-static growth in intact brittle rocks under triaxial compression in experiments that utilize AE events to monitor the faulting process. Rather than stabilize the failure process by controlling axial stress to maintain a constant rate of AE as in previous works [e.g., *Lockner and Byerlee*, 1993], we have instead developed a rapid multichannel data collection system. This enables us to elucidate the dynamics of fault nucleation using AE hypocenters under conditions of constant stress (creep) loading. These conditions are a better approximation to low strain rate condition in the Earth and allow both quasi-static and dynamic crack growth to occur. We succeeded to monitor the AE hypocenters even during unstable failure after a fault initiated in rock. In our experiments the fault initiated at a site with slight preceding damage and then propagated into the unfaulted rock with a process zone of intense cracking. This is basically in agreement with the results for Westerly granite reported by *Reches and Lockner* [1994]. *Reches and Lockner* [1994] proposed a model based on the mutual enhancement of cracking due to stress induction and pointed out the propagation of fault through the interaction of tensile cracks. However, our results, based on knowledge of the focal mechanism type, show that tensile cracking was

dominant only in the front area of the fault (process zone). When the density of the damage zone increased or when the fault growth was accelerated, shear mode or other modes containing a shear component became the major/dominant modes of cracking in agreement with a suggestion by *Cox and Scholz* [1988] based on microstructural examination.

The interaction between cracks can be quantitatively (or qualitatively) described using the *b* value, self-exciting model parameter, and focal mechanism. Interaction between cracks occurs by different mechanisms in the process and damage zones. The process zone at the front of the propagating shear fault had the following features: (1) major tensile cracking, (2) lower *b* value than background level, having fewer larger events, and (3) strong self-excitation. Thus the mechanism of crack interaction was a "mutual enhancement" or "positive feedback" on dilatation due to tensile cracking. On the other hand, the damage zone behind the process zone was characterized by (1) major shear cracking, (2) *b* value lower than background level, even lower than that in the process zone, and having more larger events, and (3) weak self-excitation. We conclude that in the damage zone, following the development of the shear fault with increasing crack density, linkage between cracks became the major mechanism of crack interaction and fault development.

The mutual changes of the *b* value and self-exciting strength seem to occur as a result of a hierarchy of fault growth, which was not observed under slowed down loading conditions [*Lockner et al.*, 1991]. Therefore our experimental results are under a more realistic approximation of the Earth's conditions and they are meaningful for the problems of earthquakes as well as rock bursts.

Acknowledgments. We thank Ian Main, Simon Cox, and Philip Meredith for their constructive reviews of this paper. This work was supported by the special fund of the Science and Technology Agency of Japan. This work was also partially supported by grant G1998040704 of the Ministry of Science and Technology of China.

References

Akaike, H., A new look at the statistical model identification, *IEEE Trans. Autom. Control, AC-19*, 716-723, 1974.

Aki, K., Maximum likelihood estimate of *b* in the formula $\log N = a - bm$ and its confidence, *Bull. Earthquake Res. Inst. Univ. Tokyo, 43*, 237-239, 1965.

Ashby, M.F., and C.G. Sammis, The damage mechanics of brittle solids in compression, *Pure Appl. Geophys., 133*, 489-521, 1990.

Brace, W.F., B. W. Paulding, Jr., and C. Scholz, Dilatancy in the fracture of crystalline rocks, *J. Geophys. Res., 71*, 3939-3953, 1966.

Cox, S.J.D., and P.G. Meredith, Crack formation and material softening in rock measured by monitoring acoustic emission, *Int. J. Rock Mech. Min. and Geomech. Abstr., 30*, 11-24, 1993.

Cox, S.J.D. and C. H. Scholz, Rupture initiation in shear fracture of rocks: an experimental study, *J. Geophys. Res., 93*, 3307-3320, 1988.

Dieterich, J.H., Earthquake nucleation on faults with rate and state-dependent friction, *Tectonophysics, 211*, 115-134, 1992.

Dieterich, J. H., and B. Kilgore, Implication of fault constitutive properties for earthquake prediction, *Proc. Natl. Acad. Sci. U.S.A., 93*, 3787-3794, 1996.

Gutenberg, B., and C. F. Richter, *Seismicity of the Earth*, 310 pp., Princeton Univ. Press, Princeton, N. J., 1954.

Horii, H., and S. Nemat-Nasser, Compression-induced cracks growth in brittle solids: Axial splitting and shear failure, *J. Geophys. Res., 90*, 3105-3125, 1985.

Johnson, A.M., R.W. Fleming, and K.M. Cruikshank, Shear zones formed along long straight traces of fault zones during the 28 June 1992 Landers, California earthquake, *Bull. Seismol. Soc. Am., 84*, 499-510, 1994.

Kato, N., K. Yamamoto, H. Yamamoto, and T. Hirasawa, Strain-rate effect on frictional strength and the slip nucleation process, *Tectonophysics, 211*, 269-282, 1992.

Kusunose, K., Fracture mechanics of rocks, *J. Phys. Earth, 43*, 479-504, 1995.

Lei, X.L., O. Nishizawa, K. Kusunose, and T. Satoh, Fractal structure of the hypocenter distribution and focal mechanism solutions of AE in two granites of different grain size, *J. Phys. Earth, 40*, 617-634, 1992.

Lei, X.L., O. Nishizawa, T. Satoh, and K. Kusunose, An AE data processing program for windows (in Japanese with English abstract), *Bull. Geol. Surv. Jpn., 48*, 447-457, 1997.

Lei, X.L., T. Satoh,, O. Nishizawa, K. Masuda, and K. Kusunose, A real time AE hypocenter monitoring system for laboratory rock fracture experiment, *Bull. Geol. Surv. Jpn., 49*.353-363, 1998.

Li, Y. G, K. J. Aki, D. Adams, A. Hasemi, and W. H. K. Lee, Seismic guided waves trapped in the fault zone of the Landers, California, earthquake of 1992, *J. Geophys. Res., 99*, 11,705-11,722, 1994.

Liakopoulou-Morris, F., I.G. Main, and B.R. Crawford, Microseismic properties of a homogeneous sandstone during fault nucleation and frictional sliding, *Geophys. J. Int., 119*, 219-230, 1994.

Lockner, D.A. and J.D. Byerlee, How geometrical constraints contribute to the weakness of mature faults, *Nature, 363*, 250-252, 1993.

Lockner, D.A., J.D. Byerlee, V. Kuksenko, A. Ponomarev, and A. Sidorin, Quasi-static fault growth and shear fracture energy in granite, *Nature, 350*, 39-42, 1991.

Main, I.G., P.G. Meredith, and C. Jones, A reinterpretation of the precursory seismic *b*-value anomaly from fracture mechanics, *Geophys. J., 96*, 131-138, 1989.

Main, I.G., P.R. Sammonds, and P.G. Meredith, Application of a modified Griffith criterion to the evolution of fractal damage during compressional rock failure, *Geophys. J. Int., 115*, 367-380, 1993.

Moore, D.E., and D.A. Lockner, The role of cracking in shear-fracture propagation in granite, *J. Struct. Geol., 17*, 95-114, 1995.

Moore, D. E., R. Summers, and J. D. Byerlee, Faults, fractures and other deformation features produced during loading of granite in triaxial equipment, *U.S. Geol. Surv. Open File Rep., 90-349*, 1990.

Nishizawa, O., and H. Noro, A self-exciting process of acoustic emission occurrence in steady creep of granite under uniaxial stress, *Geophys. Res. Lett., 17*(10), 1521-1524, 1990.

Ogata, Y., and K. Katsura, Point-process models with linearly parametrized intensity for application to earthquake data, *J. Appl. Probab., 23A*, 291-310, 1986.

Ogata, Y., H. Akaike, and K. Katsuura, The application of linear intensity model to the investigation of causal relations between a point process and another stochastic process, *Ann. Inst. Stat. Math., Part B, 34*, 373-387, 1982.

Ohnaka, M., Nonuniformity of the constitutive law parameters for shear rupture and quasi-static nucleation to dynamic rupture: A physical model of earthquake generation processes, *Proc. Natl. Acad. Sci. U.S.A., 93*, 3795-3802, 1996.

Ohnaka, M., and T. Yamashita, A cohesive zone model for dynamic shear faulting based on experimentally inferred constitutive relation and strong motion source parameters, *J. Geophys. Res., 94*, 4089-4104, 1989.

Ohnaka, M., and Y. Kuwahara, Characteristic features of local breakdown near a crack-tip in the transition zone from nucleation to dynamic rupture during stick-slip shear failure, *Tectonophysics, 175*, 197-220, 1990.

Rao, M.V.M.S., Significance of AE-based *b*-value in the study of progressive failure of brittle rock: Some examples from recent experiments, in *Proceedings of the 14th World Conference on Non-Destructive Testing*, edited by C.G. Krishnadas Nair et al., pp.2463-2467, Oxford & IOSH Publ., New Delhi, India, 1996.

Reches, Z., and D.A. Lockner, Nucleation and growth of faults in brittle rocks, *J. Geophys. Res., 99*, 18159-18173, 1994.

Sammonds, P.R., P.G. Meridith, and I.G. Main, Role of pore fluids in the generation of seismic precursors to shear fracture, *Nature, 359*, 228-230, 1993.

Satoh, T., and O. Nishizawa, A high speed, multi-channel waveform

recording system for AE measurement (in Japanese with English abstract), *Bull. Geol. Surv. Jpn.*, *48*, 439-446, 1997.

Satoh, T., K. Shivakumar, O. Nishizawa, and K. Kusunose, Precursory localization and development of microfractures along the ultimate fracture plane in amphibolite under triaxial creep, *Geophys. Res. Lett.*, *23*(8), 865-868, 1996.

Scholz, C.H., The frequency-magnitude relation of microfracturing in rock and its relation to earthquakes, *Bull. Seismol. Soc. Am.*, *58*, 399-415, 1968.

Sondergeld, C.H., and L.H. Estey, Source mechanism and microfracturing during uniaxial cycling of rock, *Pure Appl. Geophys.*, *120*, 151-166, 1982.

Sun, X., H.R. Hardy Jr., and M.V.M.S. Rao, Acoustic emission monitoring and analysis procedures utilized during deformation studies on geologic materials, in *Acoustic Emission: Current Practice and Future Directions*, edited by W. Sachse, J. Roget, and K. Yamaguchi, pp.365-380, Am. Soc. For Test. And Mater., West Conshohocken, Pa., 1991.

Utsu, T., A method for determining the value of b in a formula $\log n = a - bm$ showing the magnitude-frequency relation for earthquakes (in Japanese), *Geophys. Bull. 13*, pp.99-103, Hokkaido Univ., Hokkaido, Japan, 1965.

Zang, A., F. C. Wagner, S. Stanchits, G. Dresen, R. Andresen, and M.A. Haidekker, Source analysis of acoustic emission in Aue granite core under symmetric and asymmetric compressive loads, *Geophys. J. Int.*, *135*, 1113-1130, 1998.

K. Kusunose, X.L. Lei, and T. Satoh, Earthquake Research Department, Geological Survey of Japan, 1-1-3 Higashi, Tsukuba, Ibaraki-ken, Japan 305-8567. (lei@gsj.go.jp; kin@gsj.go.jp; saatoh@gsj.go.jp)

O. Nishizawa, Geophysics Department, Geological Survey of Japan, 1-1-3 Higashi, Tsukuba, Ibaraki-ken, Japan 305-8567. (g0192@gsj.go.jp)

M.V.M.S. Rao, National Geophysical Research Institute, Hyderabad - 500 007, India. (postmast@csngri.ren.nie.in)

(Received April 1, 1999; revised August 16, 1999;
accepted October 28, 1999.)